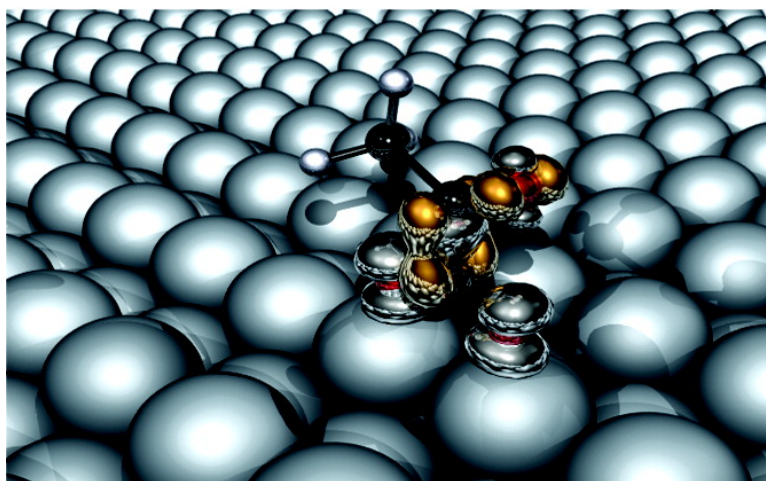**Article**

Insight into the Reduction of Pyruvic Acid to Lactic Acid over Cu{110}: The Crucial Role of Intramolecular Tunneling in Direct Hydrogenation

Glenn Jones, and Stephen J. Jenkins

More About This Article

Additional resources and features associated with this article are available within the HTML version:

- Supporting Information
- Access to high resolution figures
- Links to articles and content related to this article
- Copyright permission to reproduce figures and/or text from this article

View the Full Text HTML

Insight into the Reduction of Pyruvic Acid to Lactic Acid over Cu{110}: The Crucial Role of Intramolecular Tunneling in Direct Hydrogenation

Glenn Jones[†] and Stephen J. Jenkins*

The University of Cambridge, Department of Chemistry, Lensfield Road, Cambridge, CB2 1EW, U.K.

Received October 10, 2007; E-mail: sjj24@cam.ac.uk

Abstract: This work presents results from density functional theory calculations which are used to elucidate the reduction of pyruvic acid to lactic acid by direct hydrogenation over Cu{110} in vacuo. We propose a plausible pathway from reactants to products that crucially relies upon an intramolecular tunneling step to circumvent energetically unfavorable hydrogen exchange with the surface. The conclusions are further augmented by analyzing the electron density and frontier orbitals of key reaction intermediates. This reveals the origin of the predicted activity to be intimately linked to the electronic structure, which in turn is dependent upon the asorption geometry of pyruvic acid. Through the use of equilibrium thermodynamics, we are able to show the influence of temperature and pressure on the reaction profile. Importantly showing, that as the temperature is raised at low pressure (1×10^{-10} mbar), so the rate-determining step switches from being the carbonyl reduction to the reprotonation of the carboxylate group (leading to the desorption of lactic acid). At ambient pressure of 1 bar, the influence of temperature on the relative barrier heights is much less significant. This is an important step in attempting to bridge the so-called "pressure gap" and opens up the possibility of understanding the reactivity of small biologically relevant molecules at metal surfaces.

1. Introduction

The adsorption of biologically relevant molecules (biomolecules) at metal surfaces is an area of intense current study, as evidenced by several recent comprehensive review articles.[1-7] Specific adsorbates studied the range from large and complex molecules such as cinchonidine[8,9] or quinine,[9] through medium-sized molecules such as lepidine[9] or quinoline,[9,10] to small model molecules such as alanine,[2,11-22] lysine,[23-26] cysteine,[27-30]

and tartaric acid.[31-34] Much of the focus in these model systems has been on the relationship between the chirality of individual adsorbates and that of whole overlayers[35,33,36] or between the

† Currently based at Johnson Matthey Technology Centre, Blounts Court, Sonning Common, Reading, RG4 9NH, U.K. E-mail: gjones@matthey.com.
(1) Kasemo, B. *Curr. Opin. Sol. State Mater. Sci.* **1998**, *3*, 451.
(2) Barlow, S. M.; Raval, R. *Surf. Sci. Rep.* **2003**, *50*, 201.
(3) De Schryver, F. C.; De Feyter, S. *Chem. Soc. Rev.* **2003**, *32*, 139.
(4) Ernst, K. H. *Top. Curr. Chem.* **2006**, *265*, 209.
(5) Mallat, T.; Orglmeister, E.; Baiker, A. *Chem. Rev.* **2007**, *107*, 4863.
(6) Barlow, S. M.; Raval, R. *Curr. Opin. Colloid Interface Sci.* **2008**, *13*, 65.
(7) James, J. N.; Sholl, D. S. *Curr. Opin. Colloid Interface Sci.* **2008**, *13*, 60.
(8) Behzadi, B.; Ferri, D.; Baiker, A.; Ernst, K. H. *Surf. Sci.* **2007**, *253*, 3480.
(9) Ma, Z.; Lee, I.; Zaera, F. *J. Am. Chem. Soc.* **2007**, *129*, 16083.
(10) Bonello, J. M.; Lindsay, R.; Santra, A. K.; Lambert, R. M. *J. Phys. Chem. B* **2002**, *106*, 2672.
(11) Williams, J.; Haq, S.; Raval, R. *Surf. Sci.* **1996**, *303*, 368.
(12) Hasselström, J.; Karis, O.; Weinelt, M.; Wassdahl, N.; Nilsson, A.; Nyberg, M.; Petterson, L. G. M.; Samant, M. G.; Stöhr, J. *Surf. Sci.* **1998**, *407*, 221.
(13) Booth, N. A.; Woodruff, D. P.; Schaff, O.; Gießel, T.; Lindsay, R.; Baumgärtel, P.; Bradshaw, A. M. *Surf. Sci.* **1998**, *397*, 258.
(14) Barlow, S. M.; Kitching, K. J.; Haq, S.; Richardson, N. *Surf. Sci.* **1998**, *401*, 322.
(15) Chen, Q.; Frankel, D. J.; Richardson, N. V. *Surf. Sci.* **2002**, *497*, 37.
(16) Toomes, R. L.; Kang, J.-H.; Woodruff, D. P.; Polcik, M.; Kittel, M.; Hoeft, J.-T. *Surf. Sci.* **2003**, *522*, L9.
(17) Rankin, R. B.; Sholl, D. S. *Surf. Sci.* **2004**, *548*, 301.
(18) Rankin, R. B.; Sholl, D. S. *Surf. Sci.* **2005**, *574*, L1.
(19) Jones, G.; Jones, L. B.; Thibault-Starzyk, F.; Seddon, E. A.; Raval, R.; Jenkins, S. J.; Held, G. *Surf. Sci.* **2006**, *600*, 1924.
(20) Nyberg, M.; Odelius, M.; Nilsson, A.; Pettersson, L. G. M. *J. Chem. Phys.* **2003**, *119*, 12577.
(21) Jones, G.; Jenkins, S. J.; King, D. A. *Surf. Sci. Lett.* **2006**, *600*, L224.
(22) Gladys, M. J.; Stevens, A. V.; Scott, N. R.; Jones, G.; Batchelor, D.; Held, G. *J. Phys. Chem. C* **2007**, *111*, 8331.
(23) Humblot, V.; Methivier, C.; Pradier, C. M. *Langmuir* **2006**, *22*, 3089.
(24) Humblot, V.; Methivier, R., C.; Pradier, C. M. *Surf. Sci.* **2007**, *601*, 4189.
(25) Zhao, X. Y. *J. Am. Chem. Soc.* **2000**, *122*, 12584.
(26) Wang, W. S.; Zhao, R. G.; Zhao, X. Y. *Langmuir* **2000**, *16*, 9812.
(27) Kühnle, A.; Molina, L. M.; Linderoth, T. R.; Hammer, B.; Besenbacher, F. *Phys. Rev. Lett.* **2004**, *93*, 086101.
(28) Kühnle, A.; Linderoth, T. R.; Besenbacher, F. *J. Am. Chem. Soc.* **2006**, *128*, 1076.
(29) Greber, T.; Šljivančanin, Z.; Schillinger, R.; Wider, J.; Hammer, B. *Phys. Rev. Lett.* **2006**, *96*, 056103.
(30) Greber, T.; Hammer, B.; Šljivančanin, Z.; Schillinger, R. *Phys. Rev. Lett.* **2007**, *98*, 136102.
(31) Lorenzo, M. O.; Baddeley, C. J.; Muryn, C.; Raval, R. *Nature* **2000**, *404*, 376.
(32) Lorenzo, M. O.; Humblot, V.; Murray, P.; Baddeley, C. J.; Haq, S.; Raval, R. *J. Catal.* **2002**, *205*, 123.
(33) Humblot, V.; Lorenzo, M. O.; Baddeley, C. J.; Haq, S.; Raval, R. *J. Am. Chem. Soc.* **2004**, *126*, 6460–6469.
(34) Romer, S.; Behzadi, B.; Fasel, K. H.; Ernst, R. *Chemistry* **2005**, *11*, 4149.
(35) Chen, Q.; Richardson, N. V. *Nat. Mater.* **2003**, *2*, 324.

intrinsic chirality of the substrate and that of the adsorbate.[37,38,22] Detailed theoretical understanding of biomolecular *reaction mechanisms* at metal surfaces remains relatively lacking, however, as density functional theory (DFT) has thus far been mainly employed in establishing favored adsorption geometries and energetics. In the present work, we propose a testable reaction mechanism for the hydrogenation of pyruvic acid to lactic acid over a copper catalyst. The system is complex enough to be interesting from a biological perspective, but at the same time, simple enough to be tractable within first-principles calculations and amenable to the incisive experimental techniques of single-crystal ultrahigh-vacuum surface science. Clearly, extrapolation of such results beyond the low-pressure limit would be far from straightforward, but nevertheless, we believe that the literature supports our view that this approach remains relevant.[1–38] To a degree, arguments from thermodynamics can be brought in to help bridge the "pressure gap", and this we indeed attempt within the present work.

Pyruvic acid ($CH_3COCOOH$) is a simple alpha-keto acid that is chemically related to industrially important prochiral alpha-keto esters. The product from hydrogenation of pyruvic acid is lactic acid ($CH_3CH(OH)COOH$), a chiral molecule that bears a resemblance to the amino acid alanine studied previously by ourselves and others as an adsorbate on Cu{110}.[11–15,2,16–22] It differs from the amino acid only by the substitution of the amine group with an alcohol group, and like many amino acids, both pyruvic acid and lactic acid can be found in the human body and other living organisms.

Previous computational work on pyruvic and lactic acids has concentrated on the isolated species and includes conformational analysis coupled with infrared spectroscopy assignments.[39–46] At present, there exists only one published article regarding pyruvic acid adsorbed at a metal surface,[47] although the related alkyl pyruvates and lactates have been the subject of some previous experimental[48] and theoretical[49–51] study. The industrial reduction of alkyl pyruvates to alkyl lactates is usually carried out on a platinum or palladium catalyst employing a chiral modifier such as cinchonidine to effect enantioselectivity.[52–55,51] Despite the body of knowledge currently available, no generally accepted consensus on the mechanistic mode of action has yet been reached. It is hoped the current work will shed light on the potential reactions of pyruvic acid, as well as contributing to the much-studied but relatively little-understood alkyl pyruvate reactions.

This paper therefore presents results from fundamental adsorption structure and bonding calculations of pyruvic and lactic acid on Cu{110} and, furthermore, models the hydrogenation reaction pathway linking the two molecules. The choice of substrate is motivated in part by the existing body of knowledge for other biologically relevant adsorbates on Cu{110} and partly by its intrinsic chemical and symmetry-structure suitability for the present studies. Copper is a rather mildly reactive metal, unlikely to induce substantial dissociation of fragile biological adsorbates at moderate temperatures. The {110} surface plane, meanwhile, is the highest-symmetry stepped surface for *fcc* crystals, having two mirror planes where all others have precisely one.[56,57] The Cu{110} surface is thus a simple and amenable substrate upon which to commence studies of biological reactions.

To begin, we describe in section 2 our computational methodology and strategy. Following this, calculated energetic and geometric data for ordered overlayers of both pyruvic and lactic acid are presented in section 3, together with discussion of the general binding motifs observed. The electronic structures of the resulting geometries are qualitatively analyzed through three-dimensional visualization of individual eigenstates and electron density difference plots. Quantitative analysis is achieved through application of Bader's[58] topological approach for partitioning the electron density. In section 4, we address the reduction by direct hydrogenation of pyruvic acid to lactic acid on Cu{110}. A pathway is found along which the starting materials pass to the product via an intramolecular tunneling mechanism. It is furthermore shown that the reactivity of this process can be understood in terms of the electronic structure of the adsorbate at the rate-determining steps.

2. Methodology

2.1. Total-Energy Calculations. Results from several total-energy calculations are presented here, all of which were carried out using DFT as implemented in CASTEP computer code.[59] This approach employs Vanderbilt ultrasoft pseudopotentials[60] for electron–ion interactions and the Perdew–Wang generalized gradient approximation for exchange and correlation[61] (GGA-PW91). A plane wave basis set expanded to a kinetic energy cutoff at 340 eV describes the electronic wave functions.

Integration over the Brillouin zone was carried out using a Monkhorst–Pack[62] mesh. The bulk Cu lattice constant, for use in the surface calculations, was calculated as $a = 3.606$ Å (from a primitive unit cell applying a mesh of dimensions $7 \times 7 \times 7$). Isolated molecule structures were calculated in a $10 \times 10 \times 10$ Å³ cell containing just one molecule, sampling only the Γ-point. For

(36) Fasel, R.; Parschau, M.; Ernst, K. H. *Nature* **2006**, *439*, 7075.
(37) Ahmadi, A.; Attard, G.; Feliu, J.; Rodes, A. *Langmuir* **1999**, *15*, 2420–2424.
(38) Attard, G. *J. Phys. Chem. B* **2001**, *105*, 3158.
(39) Pecul, M.; Rizzo, A.; Leszczynski, J. *J. Phys Chem. A.* **2002**, *106*, 11008.
(40) Reva, I. D.; Stepanian, S. G.; Adamowicz, L.; Fausto, R. *J. Phys. Chem. A* **2001**, *105*, 4773.
(41) Chen, C.; Shyu, S.-F. *J. Mol. Struct. (Theochem)* **2000**, *503*, 201.
(42) Zhou, Z.; Du, D.; Fu, A. *Vib. Spec.* **2000**, *23*, 181.
(43) Dyllick-Brenzinger, C. E.; Bauder, A.; Günthard, H. *Chem. Phys.* **1977**, *23*, 195.
(44) Alsenoy, C. V.; Schäfer, L.; Siam, K.; Ewbank, J. D. *J. Mol. Struct. (Theochem)* **1989**, *187*, 271.
(45) Marstokk, K. M.; Mollendal, H. *J. Mol. Struct.* **1974**, *20*, 257.
(46) Domingo, L. R.; Andrés, J.; Moliner, V.; Safont, V. S. *J. Am. Chem. Soc.* **1997**, *119*, 6415.
(47) Yang, X.; He, Z. H.; Zhou, X. J.; Xu, S. H.; Leung, K. T. *App. Surf. Sci.* **2006**, *252*, 3647.
(48) Blaser, H.-U.; Jalett, H.-P.; Müller, M.; Studer, M. *Cat. Today* **1997**, *37*, 441.
(49) Bürgi, T.; Atamny, F.; Schlaögl, R.; Baiker, A. *J. Phys. Chem. B* **2000**, *104*, 5953.
(50) Vargas, A.; Bürgi, T.; Baiker, A. *J. Catal.* **2004**, *439*, 439.
(51) Rauls, E.; Hammer, B. *Catal. Lett.* **2006**, *106*, 111.
(52) Jannes, G.; Dubois, V. *Chiral Reactions in Heterogeneous Catalysis*; Plenum Press: New York, 1995.
(53) Collins, A. N.; Sheldrake, G. N.; Crosby, J. *Chirality in Industry: The Commercial Manufacture and Applications of Optically Active Compounds*; John Wiley: New York, 1995.
(54) Blaser, H. U.; Baiker, A. *A handbook of Heterogeneous Catalysis*; VCH Publishers: Weinheim, 1997; Vol. 5, p 2422.

(55) Baiker, A. *Cat. Today* **2005**, *100*, 159–170.
(56) Pratt, S. J.; Jenkins, S. J.; King, D. A. *Surf. Sci.* **2005**, *585*, L159.
(57) Jenkins, S. J.; Pratt, S. J. *Surf. Sci. Rep.* **2007**, *62* (10), 373.
(58) Bader, R. F. W. *Atoms in Molecules: A Quantum Theory*; Oxford University Press: New York, 1990.
(59) Payne, M. C.; Teter, M. P.; Allan, D. C.; Arias, T. A.; Joannopoulos, J. D. *Rev. Mod. Phys.* **1994**, *64*, 1045.
(60) Vanderbilt, D. *Phys. Rev. B* **1990**, *41*, 7892.
(61) Perdew, J. P.; Chevary, J. A.; Vosko, S. H.; Jackson, M. R.; Pederson, K. A.; Singh, D. J.; Fiolhais, C. *Phys. Rev. B* **1992**, *46*, 6671.
(62) Monkhorst, H. J.; Pack, J. D. *Phys. Rev. B* **1976**, *13*, 5188.

the calculation of ordered overlayer structures and energies, a range of differently sized slabs and periodicities was used; final energies were taken from calculations using eight-layer slabs with a vacuum region equivalent to eight ideal bulk {110} layers. The structures discussed were all calculated from (3×2) or (4×2) unit cells, employing $3 \times 3 \times 1$ and $2 \times 3 \times 1$ Monkhorst−Pack meshes respectively. [Initial screening of different periodicities and coverages was carried out using four-layer slabs and a less dense Monkhorst−Pack mesh. The accuracy at this level is good enough to screen out particularly high-energy structures, allowing the most stable cases to be analyzed further, in higher-quality calculations.]

For intact molecular adsorption, the definition of the heat of adsorption (ΔH_{ads}) is straightforward and may be represented as

$$-\Delta H_{ads} = E_{Cu/X} - E_X - E_{Cu} \qquad (1)$$

where E_X is the calculated energy of the adsorbate in the gas phase, E_{Cu} is the clean surface energy, and $E_{Cu/X}$ is the energy of the adsorbate-covered surface; we take as implicit that E_{Cu} and $E_{Cu/X}$ should be evaluated over the same surface unit cell, sufficient to accommodate the adsorbate X at some particular coverage. Note that, in this convention, a positive value of ΔH_{ads} indicates binding of the adsorbate to the substrate. If, however, we consider the partially dissociative adsorption of a molecule (e.g., pyruvic acid adsorbing as pyruvate, lactic acid adsorbing as lactate), we can either imagine the leaving fragment (in this case H) remaining on the surface, where ΔH_{ads} could be defined as

$$-\Delta H_{ads}^A = E_{Cu/X} + nE_{Cu/H} - E_{XH_n} - (1 + n)E_{Cu} \qquad (2)$$

or alternatively desorbing to the gas phase, in which case ΔH_{ads} is defined as

$$-\Delta H_{ads}^B = E_{Cu/X} + \frac{n}{2}E_{H_2} - E_{XH_n} - E_{Cu} \qquad (3)$$

Throughout this paper, the latter definition (ΔH_{ads}^B) is used when reporting heats of adsorption of molecules. This can be rationalized as physically meaningful for the molecules studied, where the acidic O−H bond is severed upon adsorption and the resulting H adatoms recombine to desorb as H_2 at around room temperature or above in ultrahigh vacuum conditions. At lower temperatures, or at higher hydrogen partial pressures, the ΔH_{ads}^A definition might arguably be more appropriate. It should be noted that our heats for "anionic" adsorbates are never simply referenced to a corresponding neutral form in the gas phase, because such species are often unstable. In fact, calculations on some neutral gas-phase species lacking the acidic H actually see the molecule spontaneously disintegrate. Furthermore, the anionic adsorbates are not referenced to an anionic gas-phase species, because unless there is a charged stabilizing medium the anions would only be transient. It is therefore not expected that anionic species would desorb nonrecombinatively under vacuum conditions.

In order to find transition states between stable and intermediate species, a constrained minimization approach using four-layer slabs was employed. Four layers were used primarily due to the prohibitive computational effort of using a larger slab. It is also worth mentioning in this connection that DFT typically overestimates reaction barriers, a consequence of the poor description of regions of low electron density such as are found in the stretched bonds of transition states. This effect is likely to be reduced close to the surface and one would thus expect the accuracy of surface barriers to be improved over those found in the gas phase. Nevertheless, Norskov et al.[63,64] suggest that the error can be

between 0.2 and 0.3 eV·molecule^{-1}. This is significantly greater than the errors introduced through the slab size and **k**-point sampling.

2.2. Electronic Structure Analysis. In order to analyze the electronic structure of our adsorbate systems, we have constructed three-dimensional plots of individual eigenstates lying close to the Fermi level. In addition, we have made use of electron density difference plots, illustrating the change in substrate and adsorbate charge distribution upon adsorption:

$$\Delta\rho = \rho_{Cu/X} - \rho_{Cu} - \rho_X \qquad (4)$$

In this expression, ρ represents the calculated electron density (spatial variable **r** suppressed for clarity) with subscripts representing the system in question, as in the heat expressions above. Here, however, it must be understood that all densities are calculated with those atoms present held frozen at the positions adopted in the complete adsorption system (the same is clearly *not* true when evaluating adsorption heats).

A more quantitative analysis of the electron density has also been achieved via the topological approach introduced by Bader[58] and used extensively by us to obtain insight into a wide variety of different adsorption systems.[65−76,19,21] In order to understand the electron distribution and charges upon atoms in molecules, electronic charge partitioning is employed. Within Bader's paradigm, this is achieved by defining the atom in terms of boundaries having zero normal flux in the charge density and integrating over the charge within each "atomic basin". Critical points (i.e., stationary points) in the electron density can be identified through gradient analysis; of particular interest for this paper are the so-called *bond critical points*, which are points where the curvature tensor has two negative eigenvalues and one positive. Information about the nature of the bond can be gained from the ellipticity, ϵ, defined as

$$\epsilon = \left(\frac{\lambda_1}{\lambda_2} - 1\right) \qquad (5)$$

where λ_1 and λ_2 are the negative eigenvectors of the curvature tensor at the bond critical point; a convention is taken whereby λ_1 is the negative eigenvalue of largest magnitude. The ellipticity is a measure of the local anisotropy of the electron density at the bond critical point. For a cylindrically symmetric bond (e.g., single or triple), the electron density will diminish at the same rate in both transverse directions, whereas for a double bond it will not. It is possible to use this as an indication of bond order,[58] although one ought not to overinterpret small variations as the precise results may be quite sensitive to the wider electronic environment.

2.3. Initial Structures for Geometry Minimization. A large body of published experimental[11−15,2,16−19] and theoretical[17,20,19,18,21] work exists concerning the adsorption of glycine and alanine on Cu{110}. The most recent studies of glycine adsorption, which include DFT calculations by Rankin et al.[17] and by ourselves,[21]

(63) Hammer, B.; Hansen, L. B.; Norskov, J. K. *Phys. Rev. B* **1999**, *59*, 7413.

(64) Honkala, K.; Hellman, A.; Remediakis, I. N.; Logadottir, A.; Carlsson, A.; Dahl, S.; Christiansen, C. H.; Norskov, J. K. *Science* **2005**, *307*, 555.

(65) Ge, Q. F.; Jenkins, S. J.; King, D. A. *Chem. Phys. Lett.* **2000**, *327*, 125.

(66) Jenkins, S. J.; King, D. A. *J. Am. Chem. Soc.* **2000**, *122*, 10610.

(67) Yamagishi, S.; Jenkins, S. J.; King, D. A. *J. Chem. Phys.* **2001**, *114*, 5765.

(68) Jenkins, S. J.; Peterson, M. A.; King, D. A. *Surf. Sci.* **2001**, *494*, 159.

(69) Held, G.; Braun, W.; Steinruck, H. P.; Yamagishi, S.; Jenkins, S. J.; King, D. A. *Phys. Rev. Lett.* **2001**, *87*, 216102.

(70) Yamagishi, S.; Jenkins, S. J.; King, D. A. *J. Chem. Phys.* **2002**, *117*, 819.

(71) Yamagishi, S.; Jenkins, S. J.; King, D. A. *Chem. Phys. Lett.* **2003**, *367*, 116.
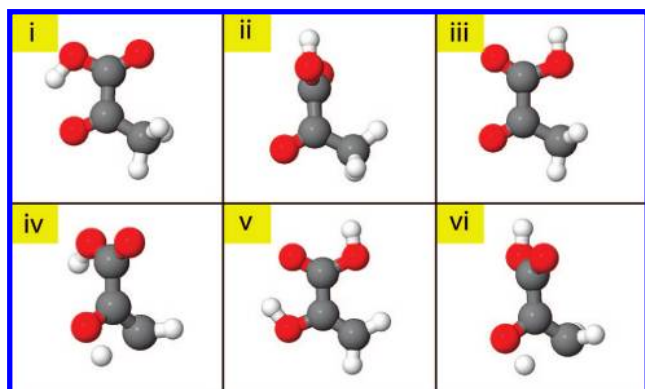
(72) Yamagishi, S.; Jenkins, S. J.; King, D. A. *Surf. Sci.* **2003**, *543*, 12.

(73) Petersen, M. A.; Jenkins, S. J.; King, D. A. *J. Phys. Chem. B* **2004**, *108*, 5909.

(74) Yamagishi, S.; Jenkins, S. J.; King, D. A. *J. Am. Chem. Soc.* **2004**, *126*, 10746.

(75) Tan, Y. P.; Khatua, S.; Jenkins, S. J.; Yu, J. Q.; Spencer, J. B.; King, D. A. *Surf. Sci.* **2005**, *589*, 173.

(76) Jenkins, S. J. *Surf. Sci.* **2006**, *600*, 1431.

Figure 1. Most stable gas-phase conformations of pyruvic acid discussed in the text: (i) trans, (ii) intermediate, (iii) cis, along with the transition states (iv and vi) linking them to (v) the enol tautomer. Relative energies are listed in Table 1. The color scheme is as follows: red = oxygen, gray = carbon, white = hydrogen. The color scheme is retained for all comparable figures in this work. Conformation i is the ground state.

Table 1. Relative Energies (eV·molecule^{-1}) of Isolated Pyruvic Acid from Figure 1[a]

geometry	present work	DFT[40]	MP2[41]
i trans	0.00	0.00	0.00
ii intermediate	0.27		
iii cis	0.25	0.18	0.14
iv transition A	3.42		
v enol	0.45		
vi transition B	3.23		

[a] Previous work at the MP2 and DFT(B2LYP) levels are quoted for comparison, and each set of data is separately referenced to its most stable conformer (the trans form in all cases).

photoelectron diffraction spectroscopy (PhD) by Woodruff and co-workers,[16,13] and combined DFT and NEXAFS by Nyberg et al.,[20] all point toward the deprotonated glycinate, in an adsorption geometry where the oxygen atoms of the carboxylate group and the nitrogen atom of the amine group are approximately atop copper atoms. The DFT studies show stable geometries in so-called hetero- and homochiral geometries with the glycinate molecule bridging between two adjacent Cu ridges. Experimental[11,77−79,19] and theoretical[18,19,21] work on adsorbed alaninate also points to the same common motif. Adsorption of lactic acid has not yet been the subject of published experimental or theoretical studies, apart from our own brief letter concerning the nature of hydrogen-bonding in the vicinity of metal surfaces.[21] Nevertheless, due to the similarity of lactic acid to alanine, it is not unreasonable to expect similar behavior. Starting geometries were therefore constructed by analogy with alaninate (i.e., considering the lactate anion in both two- and three-point binding configurations). To keep track of all the possible conformations of surface lactate, we introduce a notational system capable of capturing the relationships between chirality intrinsic to the isolated adsorbate, chirality arising from the molecule's adoption of a particular adsorption footprint, and asymmetry associated with distortion of the molecule (see the Supporting Information). In contrast, no obvious close analogue of pyruvic acid has previously been studied in detail on Cu{110} to our knowledge, so a variety of plausible geometries were devised as starting points on the basis of chemical intuition; here we focus upon only the most stable relaxed geometries that resulted.

3. Structural and Electronic Analysis

3.1. Isolated Molecules. Pyruvic acid could conceivably adopt a number of possible structures as an isolated molecule, including the so-called cis and trans conformations [Strictly speaking cis and trans isomers occur in molecules where rotation is restricted by the presence of a double bond. Here, the term is used slightly out of context but implies a similar meaning and serves as a label to differentiate between two conformations.] and their respective enol tautomers (Figure 1). In the gas phase, we find the most stable geometry to be the internally hydrogen-bonded trans form (Figure 1i) with the methyl group

arranged so as to reduce steric interactions, in keeping with previously reported results[41,40] (Table 1). The cis form (Figure 1iii) is 0.25 eV less stable. Our studies have also located another metastable conformation, in which the COOH group is rotated by approximately 90° about the C−C bond, and the total energy of this structure (Figure 1ii) is found to be only 0.02 eV higher than the metastable cis form. Calculations on a number of enol conformations have shown these species to be metastable too, with a minimum energy 0.45 eV above that of the ground state trans form. Finally, we note that the neutral pyruvic acid species can be deprotonated to form an anion, and although this is unfavorable in the gas phase (due to the absence of a solvent to stabilize the charged molecule), it is highly relevant for surface adsorption, where we have to consider the metal substrate's ability to stabilize radical or charged species.

In contrast to prochiral pyruvic acid, lactic acid is a chiral compound that, as highlighted above, closely resembles the amino acid alanine, the only difference being the exchange of the amine with the alcohol functional group. Like alanine, lactic acid is most stable in the gas phase in its neutral form, for which a number of conformers exist (Figure 2). The most stable geometry to be found through calculation is that shown in Figure 2iii (Table 2). The general trends for gas-phase stabilities are in keeping with previously reported results.[39] As with pyruvic acid, it is possible to deprotonate lactic acid to form the anionic conjugate base, lactate, which by analogy with alaninate is expected to be important for adsorption on metal surfaces even though unfavorable for the isolated molecule.

3.2. Adsorbed Pyruvic Acid and Pyruvate. At the coverages tested in our calculations, pyruvic acid was found to show a preference for adsorption in the *cis* conformation on Cu{110}, despite this geometry being less stable than the trans form in the gas phase (calculations for the enol form showed a negative heat of adsorption, implying that it is unlikely to be found on the surface). The barrier to cis−trans interconversion has not been calculated here, since the transition state is hard to locate, but it is not likely to be prohibitive at moderate temperatures.

With no experimental experience to draw upon, it was necessary to screen a wide range of possible overlayer periodicities and binding sites, although computational limitations inevitably imply that the structures tested represent only a subset of what is in fact possible. Figure 3 depicts the most stable structures found for various local coverages of cis pyruvic acid on Cu{110}, and the corresponding heats of adsorption are listed in Table 3. Inspection of the results shows an oscillatory trend when moving from low to high local coverage, with heats of adsorption increasing, decreasing, and then increasing again. As can be seen from Figure 3, there is a distinct preference for cis pyruvic acid to bridge from one close-packed Cu row to the next. The long-range order is, inevitably, harder to predict, although we note that overlayers consistent with (3 × 2) cells

(77) Polcik, M.; Allegretti, F.; Sayago, D. I.; Nisbet, G.; Lamont, C. L. A.; Woodruff, D. P. *Phys. Rev. Lett.* **2004**, *92*, 236103.
(78) Barlow, S. M.; Louafi, S.; Le Roux, D.; Williams, J.; Muryn, C.; S., H.; Raval, R. *Surf. Sci.* **2005**, *590*, 243.
(79) Sayago, D. I.; Polcik, M.; Nisbet, G.; A., L. C. L.; Woodruff, D. P. *Surf. Sci.* **2005**, *590*, 76.
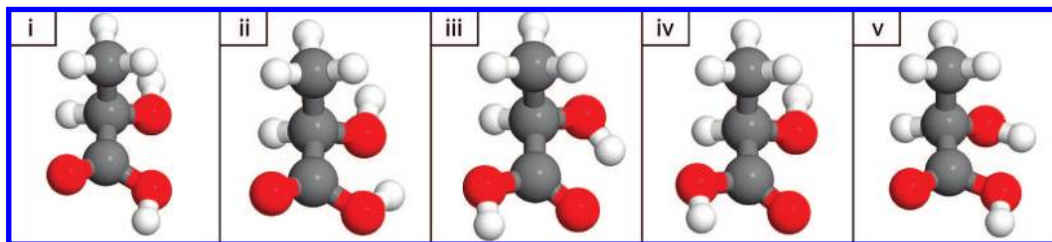
Figure 2. Lactic acid gas-phase conformations. Relative energies are shown in Table 2. Conformation iii is the ground state.

Table 2. Total Energies (eV·molecule^{-1}) of the Most Stable Isolated Lactic Acid Geometries

geometry	present work	MP2[39]
i	0.23	
ii	0.06	
iii	0.00	0.00
iv	0.23	
v	0.10	0.08

Table 3. Heats of Adsorption, ΔH_{ads}^{B} (eV·molecule^{-1}) for the Most Stable Pyruvic Acid Species[a]

unit cell	coverage (ML)	geometry	ΔH_{ads}^{B}
4 × 2	0.125	iii	0.62
3 × 2	0.167	i	0.84
4 × 2	0.250	iv(a−c)	0.66−0.69
3 × 2	0.333	ii	0.80

[a] The structures listed are shown in Figure 3.
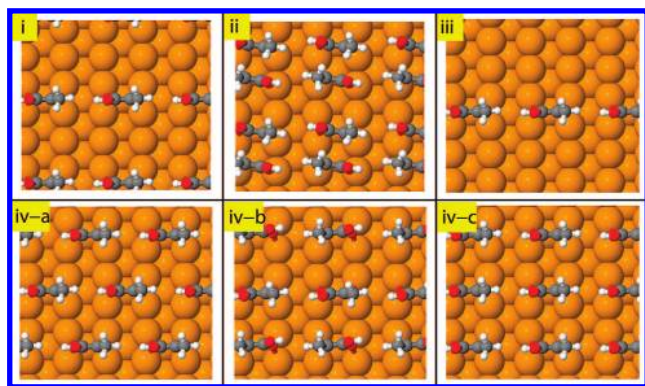
Figure 3. Diagram of the most stable pyruvic acid structures found for a given coverage. Heats of adsorption are given in Table 3.

consistently yield the higher adsorption heats in our calculations. As stated above, however, there are many permutations of the possible ordered overlayers, and many will be nearly degenerate.

An interesting aside lies in consideration of image ii in Figure 3. It can be seen that the pyruvic acid molecules pair up and that in so doing one side of the molecule is left exposed (with the other side being blocked by its partner). These pairs constitute chiral dimers; if the molecules were to pair up on the *other* side of each other then we would see a different face of each molecule exposed. In fact, what this represents is a way in which *local* molecular interactions can create a *local* chiral environment. On a strictly achiral surface, of course, there is an equal probability of *either* enantiomer of dimer being formed [That is, the symmetry (achirality) of the surface is preserved at a global level, even if it is broken locally. See ref 57 for an in-depth discussion.], although if they were to form on a chiral surface, it is possible that one would observe some measurable preference for one over the other. One might then envisage a

reaction taking place selectively at one of the exposed faces, yielding an enantiomeric excess in the product.

In contrast to cis pyruvic acid, calculations on the pyruvate anion show that it has an overriding preference for a rather different adsorption geometry, namely upright with the carboxylate oxygen atoms atop the close packed Cu rows (c.f. formate and other carboxylate species[80−83,2]). The heat of adsorption for this μ_2 species was found to vary little with coverage; for both 0.167 and 0.333 ML (one and two molecules per (3 × 2) cell, respectively), the heat of adsorption was found to be $\Delta H_{ads}^{B} = 0.82$ eV·molecule^{-1}.

In order to study the electronic structure involved in bonding pyruvic acid or the pyruvate anion to Cu{110}, representative structures at 0.167 ML coverage were examined. This coverage and periodicity were chosen to allow comparison to our reaction studies, which employ the same parameters. Of particular interest in the adsorption of pyruvic acid is the central C−C bond. In the isolated-molecule calculations this is found to have a length of 1.54 Å. Upon adsorption in the cis geometry, however, this shortens substantially to 1.39 Å, whereas the anionic and trans upright adsorption geometries show almost no change in the bond length, at 1.53 Å. This change in bond length for the cis species is indicative of an increase in bond order, borne out by findings showing the ellipticity of the bond to be 0.35 in the cis form and 0.05 when upright, as determined by topological analysis of the curvatures at the bond critical point. For reference, ellipticities of 0.20 or above are typically associated with C=C double bonds. Further evidence that there is a rearrangement of electron density is found from the electronic partitioning. Upon upright bonding of the trans form to the surface, the charges on the COOH and CO carbon atoms remain effectively unchanged relative to the gas phase (+1.5 and +1.0 e, respectively). Examination of the same carbon atoms in the cis conformation, however, reveals the positive charges to be substantially reduced from their gas-phase values (down to +1.1 and +0.6 e). Overall, one might reasonably interpret this evidence as implying transfer of electrons into the central C−C single bond of adsorbed cis pyruvic acid, yielding in effect a C=C double bond.

The electron redistribution upon adsorption of the cis form can be visualized using density difference plots (Figure 4) which can be compared to the highest occupied frontier orbital (HOFO) and lowest unoccupied frontier orbital (LUFO) of the molecule in each geometry. [The terms frontier orbital are used in this context to account for the fact that upon adsorption to the surface
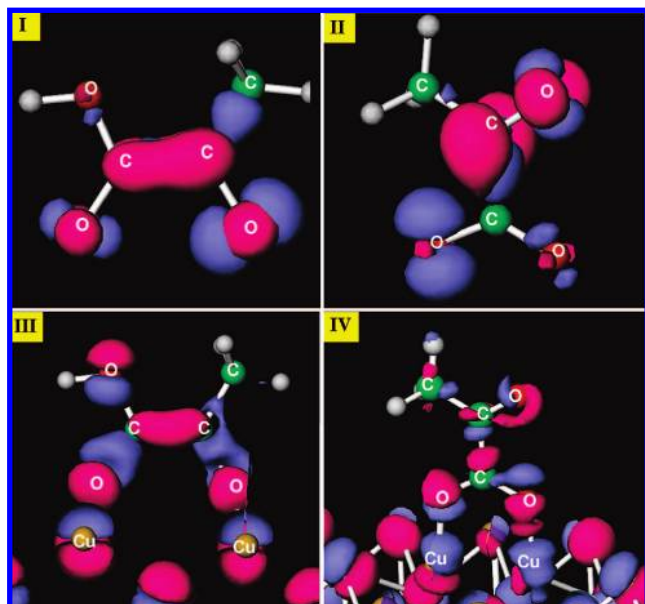
(80) Hayden, B. E.; Prince, K.; Woodruff, D. P.; Bradshaw, A. M. *Vacuum* **1983**, *33*, 876–877.

(81) Hayden, B. E.; Prince, K.; Woodruff, D. P.; Bradshaw, A. M. *Surf. Sci.* **1983**, *133*, 589–604.

(82) Sexton, B. A.; Hughes, A. E.; Avery, N. R. *Surf. Sci.* **1985**, *155*, 366–386.

(83) Puschmann, A.; Haase, J.; Crapper, M. D.; Riley, C. E.; Woodruff, D. P. *Phys. Rev. Lett.* **1985**, *54*, 2250–2252.

Figure 4. Comparison of the electron density isosurfaces (0.08 e·Å^{-3}) corresponding to the HOFO (blue) and LUFO (red) for gas-phase *cis*-pyruvic acid (I) and gas-phase pyruvate (II) with density difference plots for the adsorption of pyruvic acid cis (III) and upright pyruvate anion (IV) (electron density isosurface of blue = −0.04 and red = +0.04 e·Å^{-3}).

the orbitals are no longer localized purely on the molecule, hence the term molecular orbital would be (strictly) a misnomer.] This reveals that, upon adsorption in the neutral cis form, the LUFO is available to accept electron density; since this is predominantly a C=C π-bonding orbital, the shortening of this bond is a natural consequence. This is in contrast to the anionic form, which has no such π-bonding C=C component in its LUFO; consequently, no shortening of the bond upon adsorption would be expected or is indeed observed.

Electronic information of the type described above can yield important insights into the origin of the reactivity difference at the rate-determining steps of the two reaction pathways discussed below (section 4). Inspection of the band energies shows that for the cis form of pyruvic acid, there are no LUFOs of molecular character (within approximately 1.3 eV above the Fermi level) available to receive electrons, hence an approaching hydride species would have a large barrier to climb. However, looking at the LUFO of the upright species there *are* orbital lobes lying on both the central carbon atoms that could readily accept electrons (Figure 5). This implies that we should expect the cis form of pyruvic acid to be relatively unreactive to a negatively charged species when compared to the upright pyruvate; the reaction studies below will indeed show this to be the case. The electronic structure results show that the reactivity of pyruvic acid is very sensitive to the adsorption geometry and implies that appropriate control is required to ensure the correct form (i.e., upright pyruvate) is present on the surface for reaction to occur.

3.3. Adsorbed Lactate. Lactate at low coverages essentially exhibits two stable adsorption geometries, corresponding to two- and three-point binding motifs (μ_2 and μ_3, respectively). The μ_2 binding is similar to that of pyruvate, with the carboxylate O atop the atoms of the close-packed Cu rows. The μ_3 structure is reminiscent of that observed for alaninate and glycinate at high coverages,[2,11−21] the difference being that rather than the amine binding on the ridge opposite the carboxylate, the alcohol group does instead. The relative stability of these geometries is
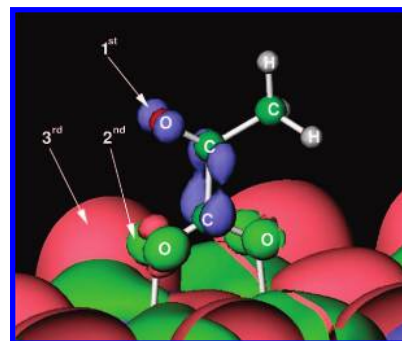
Figure 5. Lowest unoccupied frontier orbitals, extracted from the $\bar{\Gamma}$ point, for pyruvate bound upright on Cu{110}: first LUFO (+1.05 eV) blue; second LUFO (+1.08 eV) lime green; third LUFO (+1.11 eV) pink. Energies are reported relative to the Fermi level.

Table 4. Comparison of the Heats of Adsorption, ΔH^B_{ads} (eV·molecule^{-1}), of the Most Stable Low Coverage (0.167 ML) Lactate Geometries

coordination	geometry	ΔH^B_{ads}
μ_2		0.99
μ_3	R$^)$O	0.70
μ_3	OR$^($	0.83
μ_3	OR$^|$	0.77
μ_3	R$^|$O	0.71

Table 5. Comparison of the Heats of Adsorption, ΔH^B_{ads} (eV·molecule^{-1}), of the Most Stable High Coverage (0.333 ML) Lactate Geometries[a]

geometry	ΔH^B_{ads}
R$^($R$^(/$S$^)$S$^)$	1.03
R$^|$R$^|/$S$^|$S$^|$	1.11
R$^|$R$^(/$S$^)$S$^|$	1.09
R$^($R$^|/$S$^|$S$^)$	1.05
S$^)$R$^($	1.08
R$^($S$^)$	1.04
S$^|$R$^|$	1.14
R$^|$S$^|$	1.08
S$^|$R$^(/$S$^)$R$^|$	1.13
R$^($S$^|/$R$^|$S$^)$	1.05

[a] The intermolecular hydrogen-bond orientation in all cases is that depicted in image i of Figure 6.

found to vary with coverage; at a coverage of 0.167 ML, μ_2 binding is the most stable with a ΔH^B_{ads} value of 0.99 eV·molecule^{-1}, which can be compared to the most stable μ_3 model having a ΔH^B_{ads} of 0.83 eV·molecule^{-1} (Table 4). However, at 0.333 ML the μ_3 model is stabilized, with the greatest ΔH^B_{ads} exceeding 1.10 eV·molecule^{-1} (Table 5). This stablilization at higher coverage can primarily be attributed to hydrogen bonds, as demonstrated in our recently published work[21] where a topological analysis was used to provide insight into the formation of hydrogen-bonded adsorbate networks.

Although the μ_3 model of lactate can in principle form numerous different combinations of chiral and racemic overlayers with varying backbone conformations, the heats of adsorption for each of the geometries can be seen to lie within 0.08 eV·molecule^{-1} of each other (Table 5). This is just as expected based on similar calculations carried out for adsorbed alaninate and glycinate. Lactic acid does have one further complication, however, in that not only is the backbone of the molecule free to distort, but the orientation of the O−H bond can also be varied (Figure 6). In order to investigate the possible influence of the OH orientation, three representative backbone
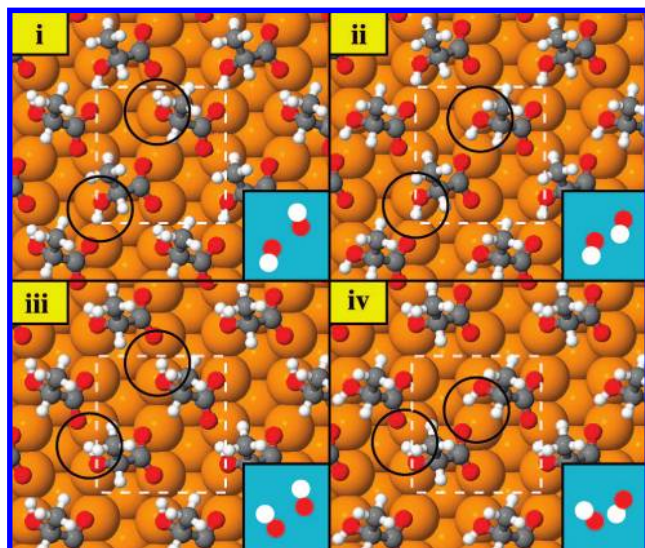
Figure 6. Diagram of H-bond orientations (highlighted by circles) within the unit cell (white square) for the lactic acid R^lR^l. Insets illustrate schematically the relative orientations of the OH moiety.

Table 6. Comparison of the Heats of Adsorption, ΔH^B_{ads} (eV·molecule^{-1}), of Three Representative Lactic Acid Anion Geometries (0.333 ML) with Different Alcohol H-Bond Orientations

geometry	ΔH^B_{ads}	OH (Figure 6)
R^lR^l/S^lS^l	1.11	i
R^lR^l/S^lS^l	1.06	ii
R^lR^l/S^lS^l	1.13	iii
R^lR^l/S^lS^l	1.06	iv
S^lR^l	1.14	i
S^lR^l	1.11	ii
S^lR^l	1.09	iii
$R^{(}S^l/R^lS^{)}$	1.05	i
$R^{(}S^l/R^lS^{)}$	1.03	ii
$R^{(}S^l/R^lS^{)}$	1.04	iii
$R^{(}S^l/R^lS^{)}$	0.99	iv

geometries (R^lR^l, S^lR^l, and $R^{(}S^l$) were chosen and a new subset of geometries with different OH orientations constructed; the ΔH^B_{ads} values were then calculated (Table 6). As can be seen, within each geometrical subset, the heat of adsorption never varies by more than 0.09 eV·molecule^{-1}; this energy difference is at the same order of magnitude as that seen between different backbone geometries. Such energy differences are sufficiently small that DFT is probably not a wholly reliable indicator of the precise adsorbate geometry in the present cases. Furthermore, it is possible that several geometries really *are* near-degenerate, so that the overlayer may rapidly interconvert between numerous subtly different configurations at room temperature.

4. Hydrogenation Reaction

The reduction of pyruvic acid to lactic acid, by direct hydrogenation on Cu{110}, has been studied as a model to test the feasibility of the process using these reactants. It is hoped that by gaining an insight into the reaction on a simple substrate, the same principles can ultimately be applied to work involving more complicated systems (including, for instance, intrinsically chiral substrates such as Cu{531}). Due to the computational demand of transition state searches, thinner slabs (four layers) were used for these quasistatic reaction calculations than for the static structural minimizations. This is not expected to alter significantly the results, bearing in mind that slab and **k**-point

Table 7. Temperature-Dependent Chemical Potentials for H_2[a]

$T(K)$	μ_{H_2} (eV) @ 10^3 mbar	μ_{H_2} (eV) @ 10^{-7} mbar	μ_{H_2} (eV) @ 10^{-10} mbar
100.00	−31.859	−32.057	−32.117
200.00	−31.973	−32.370	−32.489
298.15	−32.100	−32.692	−32.869
300.00	−32.103	−32.698	−32.877
400.00	−32.243	−33.037	−33.275
500.00	−32.390	−33.382	−33.680
600.00	−32.544	−33.735	−34.092
700.00	−32.703	−34.092	−34.509
800.00	−32.866	−34.453	−34.930
900.00	−33.033	−34.819	−35.355
1000.00	−33.204	−35.188	−35.783

[a] The units are electronvolts.

errors are in the order of hundredths of an electronvolt, whereas the accepted DFT error for reaction barriers is generally considered to be of the order of 0.2−0.3 eV·molecule^{-1}. In the previous sections, cis and trans geometries of pyruvic acid were introduced, and it was shown that the gas-phase trans form is stabilized by intramolecular hydrogen bonding and is consequently the most stable. For the present reaction studies, pathways have been investigated that begin from both cis and trans adsorption geometries.

In order to compare energies for structures having differing numbers of hydrogen atoms, we must correct calculated energies by subtraction of the chemical potential μ_H (= $\mu_{H_2}/2$). We then quote all energies relative to that of one molecule of gas-phase pyruvic acid and one (3 × 2) unit cell of clean Cu{110} (all these calculations were performed within just such a unit cell and featured precisely one $C_3O_3H_n$ species). We thus plot corrected energies E', defined as

$$E_{C_3O_3H_{n'}} = E_{C_3O_3H_n} - E_{pyr} - E_{Cu} - (n-4)\mu_H \quad (6)$$

with $E_{C_3O_3H_n}$ being the total energy per supercell of the particular surface intermediate or transition state in question and n_H being the number of hydrogen atoms involved in its structure; E_{pyr} is the energy of a gas-phase pyruvic acid molecule, and E_{Cu} is the energy of a (3 × 2) supercell of clean Cu{110}.

The necessary chemical potential is, of course, a function of the temperature and pressure of gas-phase hydrogen. We obtain μ_{H_2} via

$$\mu(T,p) = \frac{1}{N_A}(H(T,p) - TS(T,p)) \quad (7)$$

where N_A is Avogadro's number. The molar enthalpy $H(T, p^0)$ and molar entropy $S(T, p^0)$ of molecular hydrogen at standard pressure, p^0, may be taken from reference sources,[84] and the pressure dependence of the chemical potential is given by

$$\mu(T,p) = \mu(T,p^0) + kT \ln(p/p^0) \quad (8)$$

in which p is the partial pressure of hydrogen above the surface. In this manner, we find the chemical potential values listed in Table 7. Reaction pathways described below have been calculated for three situations: first, a low-pressure regime, corresponding to ultrahigh vacuum conditions with a partial pressure for H_2 of 1×10^{-10} mbar, second, a medium-pressure regime, corresponding to typical hydrogen dosing conditions (i.e., 1×10^{-7} mbar), and third, a high-pressure regime, corresponding to atmospheric pressure of H_2 (i.e., 1×10^3 mbar).

(84) Lide, D. R. *Handbook of Chemistry and Physics*, 78th ed.; CRC Press: Boca Raton, 1997.
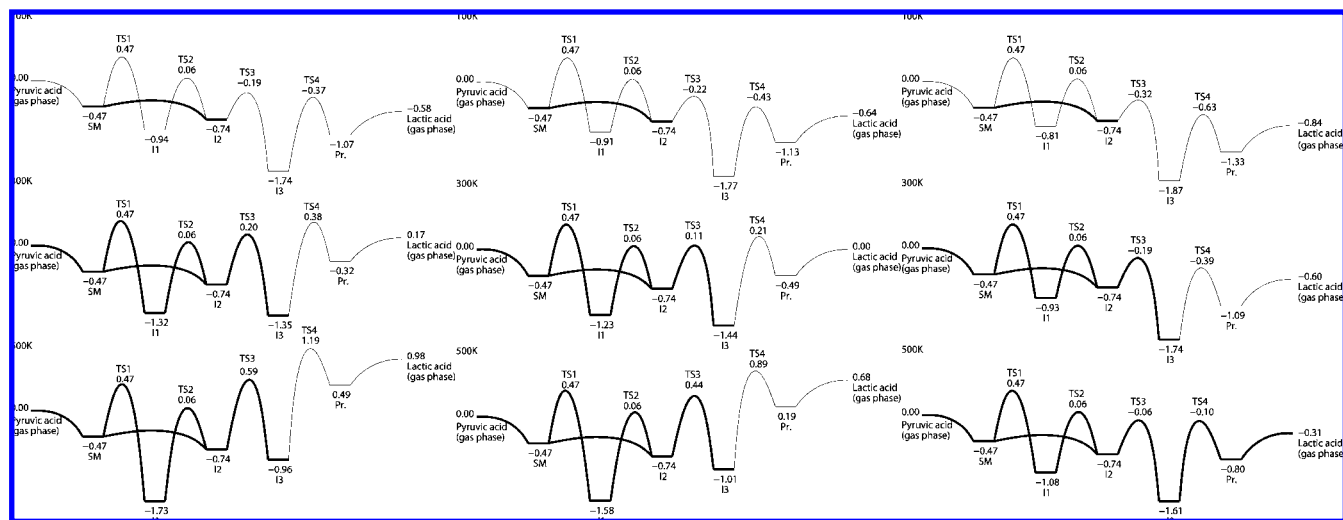
Figure 7. Pathway for hydrogenation of pyruvic acid from the trans adsorption geometry, calculated for hydrogen partial pressures of 1×10^{-10}, 1×10^{-7}, and 1×10^3 mbar (left, middle, and right panels, respectively). To provide a guide to the eye, we note that barriers of 0.32, 0.96, and 1.60 eV would be surmounted (at 100, 300, and 500 K, respectively) at a rate of approximately one event per molecule per one hundred seconds (assuming a pre-exponential factor of 10^{14} s^{-1}; states accessible by a population starting at SM *without* passing over any higher barriers are shown in bold.
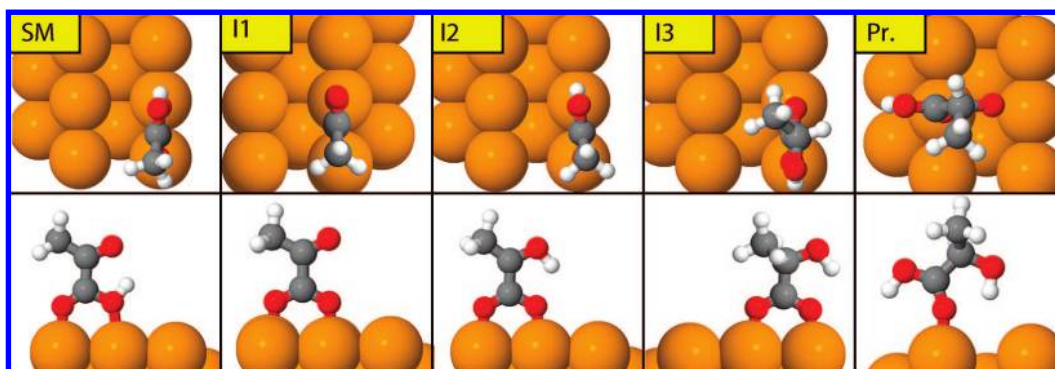

Figure 8. Structures of the adsorbed starting material (SM), intermediates (I1−3), and product (Pr) for hydrogenation of the *trans*-pyruvic acid.

Although the cis form of pyruvic acid is more stable on the surface than the trans form, we find that it is essentially unreactive toward hydrogenation. For all combinations of temperature and pressure in the ranges covered by Table 7, the lowest free energy barrier for the first reaction step (where the carbonyl C atom of adsorbed cis pyruvic acid acquires a single H atom from the surface) is never less than 2.80 eV. We do not, therefore, believe it is useful to present details of the full reaction mechanism for the cis species here.

The trans form of pyruvic acid, on the other hand, is rather more promising, and Figure 7 illustrates the reaction steps for the hydrogenation of pyruvic acid to lactic acid from this starting species. When considering the approach of the trans pyruvic acid to the surface, two scenarios can be envisaged. The first sees the pyruvic acid binding intact, then losing its acidic H to the surface, to give intermediate 1 (I1). This is followed by the sequential addition of hydrogen to the carbonyl oxygen and then the carbonyl carbon, going from intermediate 2 to intermediate 3 (I2 → I3). This leaves the anionic lactate (I3) that must gain another hydrogen atom from the surface to form the desired product, adsorbed lactic acid (Pr). The second route involves a different first step, where the trans pyruvic acid binds to the surface and there is an internal hydrogen transfer from the acid group to the carbonyl oxygen. This scenario eliminates the need for passing through transition states TS1 and TS2 (see Figure 9; among the highest barriers in the formation of adsorbed

lactate) and hence would be preferred. This step has such a low barrier, and the hydrogen atom travels such a short distance, that it may in fact be facilitated by quantum mechanical tunneling.

On the basis of our calculations, we suggest that the molecule will indeed not lose a hydrogen atom to the surface, but will instead undergo an internal protonation of the carbonyl group. This step is extremely significant, since conventional carbonyl chemistry usually requires a protic or a Lewis acid to "activate" the carbonyl carbon by binding to the carbonyl oxygen. [This means the reaction is acid catalyzed; we can consider the internal H transfer as acid catalysis due to the acid group being regenerated upon formation of the reaction product, lactic acid.] What we find here in the absence of solvent, reagent, or external acid catalyst, is that the activation is still possible via the internal transfer mechanism. Through application of the following formula, a quantum mechanical tunneling rate for the proton transfer can be calculated, where $D(E)$ is the tunneling probability, ΔE is the barrier height, and Δx is the barrier width (taken as the OH bond length). Multiplying $D(E)$ by the attempt frequency (the vibrational stretching frequency of O−H for this reaction, assumed as 10^{14} Hz) will provide an estimate for the tunneling rate. In this particular case, the tunneling rate would be appreciable (Table 8) and, in fact, dominant up to at least 500 K. The fact that tunneling does play a role suggests that it should be possible to experimentally isolate the tunneling
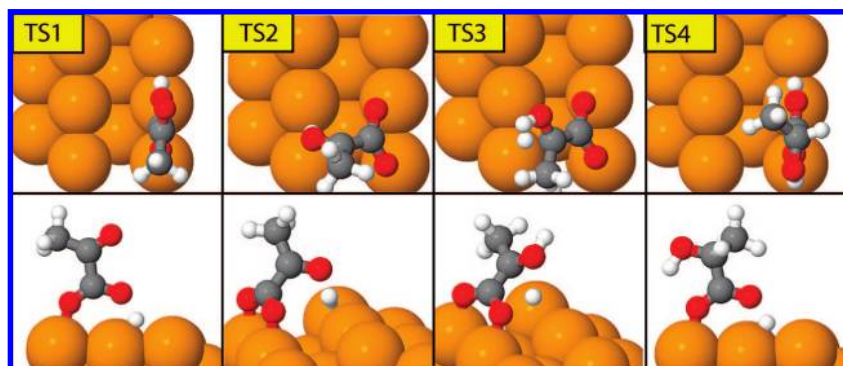
Figure 9. Structures of the transition states (TS1−4) for hydrogenation of the *trans*-pyruvic acid.

Table 8. Forward and Backward Reaction Rates for the Internal Hydrogen Transfer Step

thermal rate/K	forward rate/s^{-1}	backward rate/s^{-1}
50	7.8	4.8×10^{-27}
100	2.8×10^7	6.9×10^{-7}
300	6.5×10^{11}	1.9×10^7
400	2.3×10^{12}	9.1×10^8
500	4.9×10^{12}	9.3×10^9
QM rate	1.8×10^{13}	1.3×10^9

product at very low temperatures where thermally accessible pathways will not be populated, allowing the species to be characterized. The I2 → I3 reaction could then be induced in a controlled fashion. This significant step is, in fact, the critical point at which introduction of the chiral center is achieved. Future work under chiral conditions can potentially benefit from identification of this fact.

Viewing the pathway as a whole (Figure 7), we can make predictions regarding the different surface species that might exist under different conditions of temperature and pressure. At 100 K, for example, we might note that free energy barriers in excess of 0.32 eV would be surmounted at a rate slower than 10^{-2} events per molecule per second, which we will take arbitrarily as the boundary between "fast" and "slow" processes. Thus, rapid equilibration would only be possible between states linked by barriers less than 0.32 eV. Imagining initial conditions where the only surface species is the "starting material" (SM), the system would rapidly establish an equilibrium between SM and I2, favoring the latter at all pressures of gas-phase hydrogen. Other surface intermediates and products would be inaccessible within a short time frame.

At 300 K, the picture changes somewhat, since a free energy barrier of 0.96 eV now becomes the (somewhat arbitrary) boundary between fast and slow. Indeed, at all three indicative pressures depicted in Figure 7, states SM, I1, I2, and I3 (see Figure 8) are all readily accessible, together with desorption of pyruvic acid. At all three pressures, the equilibrium would eventually favor I3, although under ultrahigh vacuum conditions the preference over I1 would be marginal and probably outside the reliability of DFT to confidently predict.

At 500 K, the critical free energy barrier, delimiting fast and slow processes, increases to 1.60 eV. At hydrogen pressures of 1×10^{-10} and 1×10^{-7} mbar, the same range of states remains accessible as at 300 K, but the equilibrium has shifted to favor I1 over I3. At atmospheric pressure of hydrogen, however, the full range of states, including adsorbed and desorbed lactic acid becomes readily accessible; equilibrium favors I3 on the surface, but some desorption of the product material will likely occur.

To summarize, for the trans pathway, the reaction proceeds through the initial deprotonation of the carboxylic acid and internal activation of the ketone carbonyl oxygen (SM → I2), promoting the corresponding carbon to attack from a surface hydride species (H charge on surface approximately −0.3 e); importantly, attack of the carbonyl carbon (I2 → I3) is more favorable than the reprotonation of the carboxylic acid group by 0.14 eV. The subsequent step (I3 → Pr) proceeds via addition to the ketone carbonyl carbon, leaving the anionic lactate upright on the surface. Without the tunneling-assisted low-barrier pathway between SM and I2, the reaction could not proceed beyond adsorbed pyruvate (I1) for nearly all temperature and pressure combination considered here.

It is possible when carrying out hydrogenation reactions of carbonyl compounds to over-reduce the reactant. To test whether this would be the case here, the possiblity of the addition of subsequent hydrogens, culminating in the loss of a water molecule, was investigated. It was found that the starting geometry of the calculation for a species with a doubly protonated ketone oxygen saw the extra hydrogen relax onto a carboxylate oxygen. We were, furthermore, unable to locate a transition state for addition of a second H to the ketone oxygen. This leads us to conlude that over-reduction should not be a problem.

5. Conclusion

In this work, we have applied DFT to gain insight into a possible mechanism for hydrogenation of pyruvic acid to lactic acid on Cu{110}. The adsorption geometries of both molecules have been studied, showing general binding schemes for pyruvic acid and allowing comparison to previous work on glycinate and alaninate for lactic acid. In particular, for the 0.333 ML lactate structures, the μ_3 binding and hydrogen-bond-stabilized overlayer bear a striking resemblance to alaninate. The possibility of an upright μ_2 binding model at low coverage is similar to that reported for experiments conducted with glycinate.[2] Using Cu{110} as a model for the hydrogenation of pyruvic acid has given insight into the influence of structure and bonding upon reactivity, in particular the observed deactivation of the cis form of pyruvic acid to hydrogenation. This is contrary to the behavior predicted for methyl-pyruvate on Pt{111},[49] where despite the step being rate determining it is not prohibitive. Given that the cis form of pyruvic acid is predicted to be the most stable on the surface, one might believe this to be a major obstacle to hydrogenation over Cu{110}. Since the dominant gas-phase form of pyruvic acid is trans, however, we expect at least a transient population of that species on the surface, and it is through this alone that appreciable reactivity may be

achieved. Our work further indicates that tunneling-assisted internal hydrogen transfer is a critical step in the reaction mechanism, providing a low-energy pathway for activation of the ketone carbonyl oxygen toward attack by surface hydride species.

In considering the connection between ultrahigh vacuum (uhv) studies and possible practical catalysis, interesting questions for further research might include the role of potential solvents, such as water. Methods capable of addressing such questions are not, however, developed sufficiently at present to enable their routine use in plane wave DFT at realistic extended surfaces (as distinct from small-scale cluster calculations, for instance). In principle, strategies for including solvation could involve treating the solvent as a dielectric medium capable of modeling polarization and the stabilization or otherwise of charged intermediates; alternatively, one might make use of classical molecular mechanics to model solvent molecules, restricting quantum mechanics to the substrate and adsorbate; or finally, and most expensively, one could explicitly include solvent molecules within a first-principles molecular dynamics simulation of the entire system. Moves toward this end have indeed been made in some recent work by Ghiringhelli et al.,[85] where three water molecules were included in calculations of alanine adsorption at the Ni{111} surface. Although their work utilized classical molecular dynamics to obtain reasonable geometries for study, the DFT calculations were simply static geometry optimizations, hence the ability to describe dynamic and/or entropic solvent effects is lost. Doubtless solvated models of biomolecules at surfaces will become increasingly sophisticated in time, but intriguing though these possibilities are, none are readily applicable at the present time. We therefore restrict ourselves to some qualitative speculation about the role of solvents, based upon the principles of known homogeneous chemistry.

We proceed by recognizing the classification of solvents as polar/nonpolar and protic/aprotic. In the presence of a nonpolar solvent, we might reasonably expect the behavior to be little changed from our vacuum results, since possible charged intermediates would not be screened by the solvent. Polar aprotic solvents, in contrast, might have a notable effect by stabilizing charged intermediates that are not possible under vacuum conditions; a dielectric medium would be an adequate model for such a solvent, since screening is the dominant physical effect that must be described. Finally, the case of a polar protic solvent would be most challenging, requiring not only electrostatic contributions to the overall energy, but also the formation of hydrogen bonds and possible proton exchange between solvent and adsorbate. The latter effect could conceivably block activation of the carbonyl carbon via internal proton transfer, in the event that the solvent is more acidic than pyruvic acid. In conclusion, the present studies provide a benchmark for hydrogenation of pyruvic acid over Cu{110} in the absence of solvent, against which the various effects of different kinds of solvent might be measured. Moreover, the dry surface chemistry of biomolecules on metals remains a vibrant and important field in its own right, and our calculations suggest experimental conditions that could be employed in the immediate future to explore reactions connecting prochiral and chiral adsorbates deposited from the gas phase.

Supporting Information Available: Full explanation of the notation used to describe the adsorption gemetry of the lactate molecules on the surface. This material is available free of charge via the Internet at http://pubs.acs.org/.

JA077786M

(85) Ghiringhelli, L. M.; Schravendijk, P.; Site, L. D. *Phys. Rev. B* **2006**, *74*, 035437.